

LETTERS

Directional water collection on wetted spider silk

Yongmei Zheng^{1*}, Hao Bai^{2*}, Zhongbing Huang³, Xuelin Tian³, Fu-Qiang Nie³, Yong Zhao³, Jin Zhai¹ & Lei Jiang³

Many biological surfaces in both the plant and animal kingdom possess unusual structural features at the micro- and nanometre-scale that control their interaction with water and hence wettability^{1–5}. An intriguing example is provided by desert beetles, which use micrometre-sized patterns of hydrophobic and hydrophilic regions on their backs to capture water from humid air⁶. As anyone who has admired spider webs adorned with dew drops will appreciate, spider silk is also capable of efficiently collecting water from air. Here we show that the water-collecting ability of the capture silk of the cribellate spider *Uloborus walckenaerius* is the result of a unique fibre structure that forms after wetting, with the ‘wet-rebuilt’ fibres characterized by periodic spindle-knots made of random nanofibrils and separated by joints made of aligned nanofibrils. These structural features result in a surface energy gradient between the spindle-knots and the joints and also in a difference in Laplace pressure, with both factors acting together to achieve continuous condensation and directional collection of water drops around spindle-knots. Submillimetre-sized liquid drops have been driven by surface energy gradients^{7–9} or a difference in Laplace pressure¹⁰, but until now neither force on its own has been used to overcome the larger hysteresis effects that make the movement of micrometre-sized drops more difficult. By tapping into both driving forces, spider silk achieves this task. Inspired by this finding, we designed artificial fibres that mimic the structural features of silk and exhibit its directional water-collecting ability.

Spider silk, which is composed of humidity-sensitive^{11–16} hydrophilic flagelliform proteins^{17,18}, enjoys a high reputation as a fibre with excellent mechanical properties^{11,13–15,17–20}. Another intriguing but less studied feature is its ability to collect water from humid air (see Supplementary Fig. 1). This is seen in webs built by cribellate spiders, which use a cribellum—a comb-like device—to separate silk fibres drawn from their spinnerets into many exceedingly fine fibres. The environmental scanning electronic microscopy (SEM) images of the spider silk in Fig. 1 illustrate its structure. Puffs composed of nanofibrils are spaced along two main-axis fibres with a periodicity of $85.6 \pm 5.1 \mu\text{m}$ (Fig. 1a)²⁰. The puffs’ diameter is $130.8 \pm 11.1 \mu\text{m}$, and they are separated by joints with a diameter of $41.6 \pm 8.3 \mu\text{m}$. The zoomed-in image in Fig. 1b shows the puffs to be composed of random nanofibrils (20–30 nm in diameter). These highly hydrophilic nanofibrils^{17,18} enhance the wettability of spider silk, which is favourable for condensing water drops.

When dry spider silk is placed in fog, its structure changes as water starts to condense and form drops that move along the silk fibre (Fig. 2). At the initial stage, tiny water drops (black dots indicated by arrows in Fig. 2a) condense on the semitransparent puffs. As water condensation continues, the puffs shrink into opaque bumps (Fig. 2b, c) and finally form periodic spindle-knots (Fig. 2d). The impact of fog on the mechanical properties of spider silk has been noted before^{15,16}, and the present observations indicate that in the case of

cribellate spider silk, the material changes its fibre structure as a result of wetting. After this ‘structural wet-rebuilding’, directional water collection starts.

To analyse this process, images of the wet-rebuilt spider silk are divided into four regions that each contain one joint (that is, regions I, II, III and IV in Fig. 2d–f). When exposed to mist, small water drops (identified by numbers 1 to 10 in Fig. 2e) randomly condense on joints (drops 1, 3, 4, 5, 8 and 10) and on spindle-knots (drops 2, 6, 7 and 9). As water condensation continues, the drops grow in size and those on joints move directionally to the nearest spindle-knots (white arrows in Fig. 2e) where they coalesce to form larger water drops (Fig. 2f). Drops 1–5, which formed in regions I and II, coalesced into

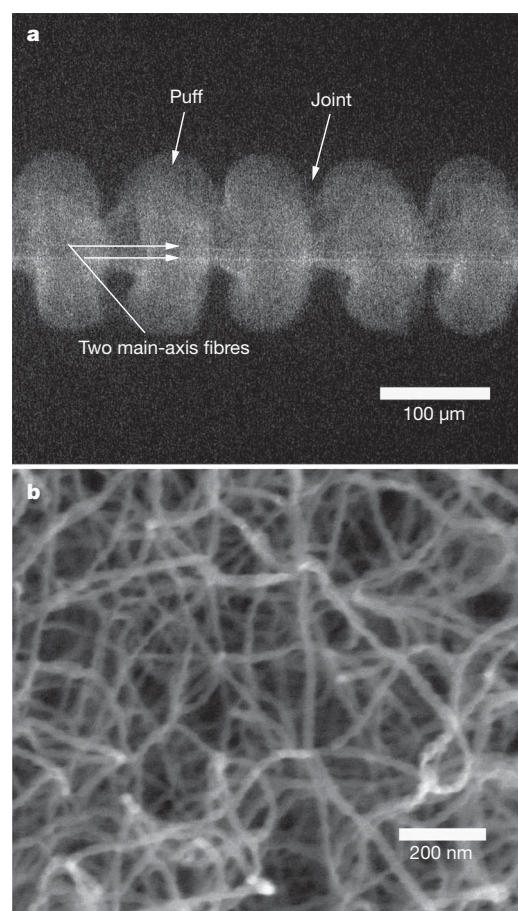


Figure 1 | Structures of dry capture silk of cribellate spider. a, Low-magnification environmental SEM image of periodic puffs and joints surrounding two main-axis fibres. **b**, Magnified image of puff composed of countless nanofibrils.

¹School of Chemistry and Environment, Beijing University of Aeronautics and Astronautics, Beijing 100191, China. ²National Center for Nanoscience and Technology, Beijing 100190, China. ³Beijing National Laboratory for Molecular Sciences (BNLMS), Institute of Chemistry, Chinese Academy of Sciences, Beijing 100190, China.

*These authors contributed equally to this work.

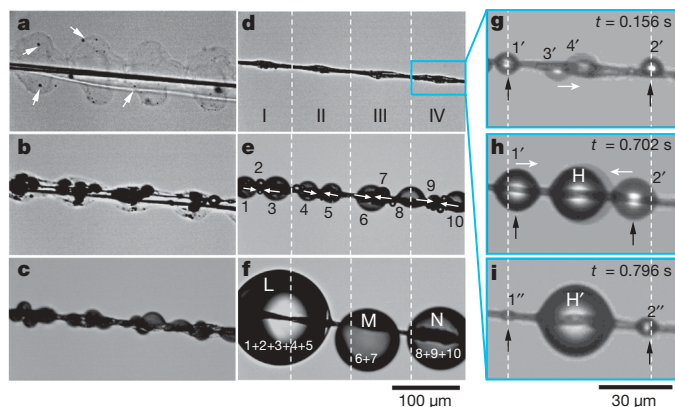


Figure 2 | *In situ* optical microscopic observation of directional water collection on spider silk in mist. **a**, Dry spider silk is of four semitransparent puffs. In mist, few tiny water drops (indicated by arrows) first condense on puffs. **b–d**, Puffs shrink to opaque bumps with water condensing and form spindle-knots linked by joint. **d–f**, The directional water collection on the wet-rebuilt multistructured spider silk. The images are divided into four regions (I, II, III and IV). **e**, Smaller water drops condense on spider silk (denoted 1–10). Water drops move directionally from joints to spindle-knots (as indicated by arrows) with volume increasing. **f**, The growing water drops 1–5 coalesce to a larger water drop L covering two spindle-knots (I and II), while water drops 6, 7 and 8–10 coalesce to two medium water drops: M covering single spindle-knot III and N covering single spindle-knot IV. **g–i**, More detailed directional drop movement on individual spindle-knot. Smaller water drops (1', 2', 3' and 4') first randomly condense on the spindle-knot and the joints at 0.156 s (**g**). With volume increasing, droplets 3' and 4' coalesce into water drop H on the spindle-knot at 0.702 s, while water droplets 1' and 2' spontaneously move from joints to spindle-knot (as indicated by white arrows) (**h**) and coalesce to a larger water drop H' on the spindle-knot at 0.796 s (**i**). Then the joints refresh and a new directional water collection cycle starts (two tiny water drops 1'' and 2'' recondense on the joints) (**i**). The black arrows indicate the condensing sites of joints that are favourable for continuous directional water collecting.

a larger drop L that covers two spindle-knots, while drops 6 and 7 in region III and drops 8–10 in region IV coalesced to form medium-sized drops M and N, each covering a single spindle-knot. Overall, these observations imply that the periodic fibre structure of spindle-knots and joints found in wetted spider silk plays a part in directional water collection.

We further monitored water collection by focusing on an individual spindle-knot of the spider silk fibre (Fig. 2g–i). In the initial stage, small water drops 1', 2', 3' and 4' randomly condensed on the spindle-knot and the two adjacent joints (Fig. 2g). The growing drop 3' then moved to the spindle-knot (white arrow in Fig. 2g) where it encountered drop 4' and coalesced to form drop H (Fig. 2h). Meanwhile, the growing drops 1' and 2' located on the joints also moved towards the spindle-knot (white arrows in Fig. 2h) and coalesced with the already-present drop H to form a larger drop H' (Fig. 2i). A rather large water drop finally formed on the spindle-knot through sequential coalescence of smaller drops originating from the joints.

In this process, the spindle-knot serves in the initial stage as a condensing site and then as a drop collecting site for the coalescence of smaller drops that originate from the joints. In contrast, the joints mainly act as condensing sites (black arrows in Fig. 2g–i), where water condenses into drops that are then transported to the spindle-knot. Importantly, after water drops have left the joints and been collected on the spindle-knot, a new cycle of water condensation and directional drop movement can start on the joints. This is seen in Fig. 2i, in which drops 1'' and 2'' condense on the joints after drops 1' and 2' have formed and moved to the spindle-knot. Taken together, these images illustrate how the cooperation between joints acting as condensing sites and spindle-knots acting mainly as collecting sites enables uninterrupted directional water

collection (see also Supplementary Fig. 2 and Supplementary Movie 1). We observed such directional water collection behaviour only with wetted silk fibres (that is, wet-rebuilt silk) from the cribellate spider *Uloborus walckenaerius*; in contrast, silkworm silk and nylon fibres with a uniform structure did not exhibit the directional water collection phenomenon (Supplementary Figs 3, 4).

To explore in more detail the role of fibre structure in directional water collection behaviour, we show, in Fig. 3, environmental SEM images of the wet-rebuilt spider silk. The wetted spider silk is composed of alternate spindle-knots and joints (apex angles $2\beta \approx 19^\circ$) with periodicity of $89.3 \pm 13.5 \mu\text{m}$ (Fig. 3a). The diameters of spindle-knots and joints are $21.0 \pm 2.7 \mu\text{m}$ and $5.9 \pm 1.2 \mu\text{m}$, respectively. Magnified images of a spindle-knot (Fig. 3b, c) reveal highly random nanofibrils that give a rough surface topography, while comparable images of a joint (Fig. 3d, e) show that it is composed of nanofibrils that run relatively parallel to the silk fibre axis and form an anisotropic aligned and relatively smooth topography. These structural features can give rise to a surface energy gradient and a difference in Laplace pressure, which can both act as a driving force for the directional movement of water drops as detailed below (see also Fig. 4).

Surface energy gradients can arise from differences in either surface chemical composition^{7,8} or surface roughness^{21,22}, and such gradients will drive water drops towards the more wettable region with a higher surface energy. According to Wenzel's law²³:

$$\cos \theta_w = r \cos \theta \quad (1)$$

where r is surface roughness, θ_w and θ are the apparent and intrinsic contact angles on rough and smooth surfaces, respectively. As for hydrophilic spider silk^{17,18}, its chemical composition does not change much along the fibre, but the joint has a smaller axial-parallel roughness and hence larger water contact angle than the spindle-knot

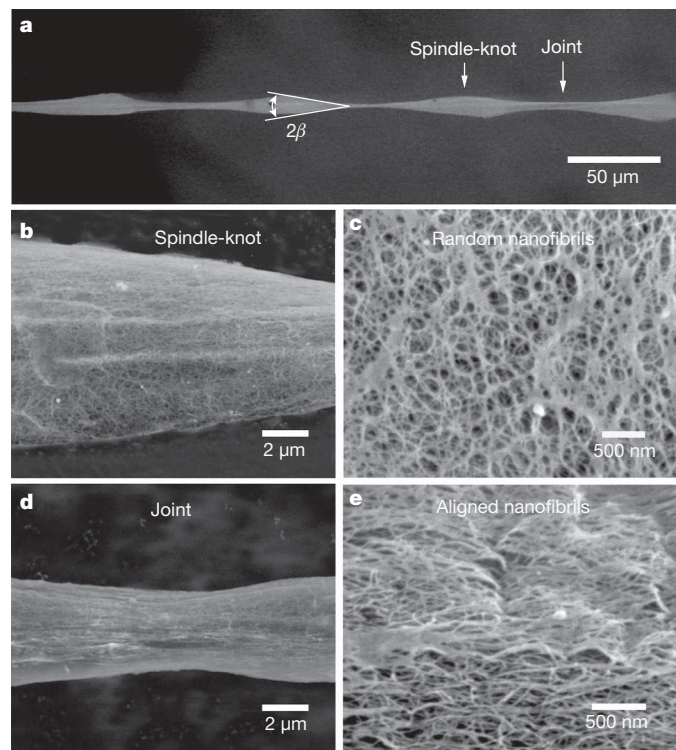


Figure 3 | Structure of wet-rebuilt spider silk. **a**, Environmental SEM images of periodic spindle-knots linking with slender joints. The apex angle of spindle-knots (2β) is about 19° . Low-magnification (**b**) and zoomed (**c**) images show that the spindle-knot is randomly interweaved by nanofibrils. **d**, **e**, Low-magnification (**d**) and high-magnification (**e**) images of the joint, which is composed of nanofibrils aligned relatively parallel to the silk axis.

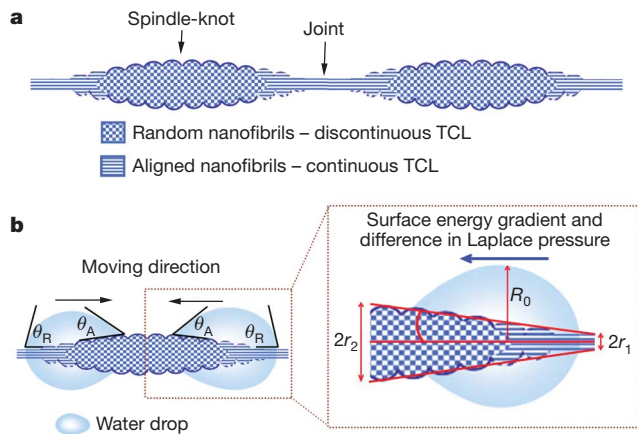


Figure 4 | Mechanism of directional water collection on wet-rebuilt spider silk. **a**, Spindle-knots are interweaved by highly random nanofibrils, while joints are composed of relatively aligned nanofibrils. Spindle-knots are of larger silk-axial roughness than joints. Meanwhile, random surface topography of spindle-knots forms discontinuous TCL, while aligned surface topography of joints forms continuous TCL for water drops, which is helpful for water drops' movement along joints. **b**, Surface structural anisotropy generates a surface energy gradient so that spindle-knots possess higher apparent surface energy than joints. At the same time, the conical shape of the spindle-knot generates a difference in Laplace pressure from the high-curvature region (joint) to the low-curvature region (spindle-knot), as the inset shows. The cooperation of these two factors drives water drops from joint to spindle-knot. The arrows denote the directions of drop movement.

(Fig. 3c, e). That is, the spindle-knot is more hydrophilic and has a higher apparent surface energy than the joint²⁴ (see also Fig. 4b). The force generated by a surface energy gradient that arises from a difference in surface roughness is given by^{7,8}:

$$F = \int_{L_j}^{L_k} \gamma (\cos \theta_A - \cos \theta_R) dl \quad (2)$$

where γ is the surface tension of water, θ_A and θ_R are the advancing and receding angles of water drop on spider silk ($\theta_A < \theta_R$, according to equation (1)), respectively, and dl is the integrating variable along the length from the joint (L_j) to the spindle-knot (L_k). The surface energy gradient arising from differences in roughness will thus drive water drops to move from the less hydrophilic region (joint with relative lower surface energy) to the more hydrophilic region (spindle-knot with high surface energy) (Fig. 4b).

The second possible driving force for directional water drop movement arises from the spindle-shaped geometry of the knots, which will generate a difference in Laplace pressure. As illustrated in Fig. 4b, a spindle-knot can be thought of as two oppositely curved and joined conical objects (inset of Fig. 4b). Such a conical shape with a curvature gradient will give rise to a difference in Laplace pressure (ΔP) acting on a water drop¹⁰:

$$\Delta P = - \int_{r_1}^{r_2} \frac{2\gamma}{(r+R_0)^2} \sin \beta dz \quad (3)$$

where r is the local radius, R_0 is the drop radius ($R_0 = (3V/4\pi)^{1/3}$, with V the drop volume), β is the half apex-angle of the spindle-knot, and z is the integrating variable along the diameter of the spindle-knot. The Laplace pressure on the high curvature site (the joint with local radius r_1) is larger than that on the low-curvature site (the spindle-knot with local radius r_2) because r_1 is smaller than r_2 , and the resultant non-equilibrium Laplace pressure difference within a water drop will propel the drop to move from the joint to the spindle-knot. The overall result is that the surface energy gradient arising from the anisotropic surface structures and the difference in Laplace pressure arising from the conical spindle-knot geometry

act cooperatively to drive condensing and growing water drops from the joint to the spindle-knot (Fig. 4b).

We observe water drops with diameters of 5–20 μm move until they coalesce and are collected on a spindle-knot (Supplementary Fig. 2). We note that the movement of sub-millimetre-sized liquid drops driven by either surface energy gradients^{7–9} or by differences in Laplace pressure¹⁰ has been realized before. But either driving force on its own has not yet been shown to move smaller drops with diameters on the micrometre scale, where contact hysteresis effects are increasingly important (see also Supplementary Discussion regarding minimum drop size). This makes it particularly interesting that the unique structural features of wet-rebuilt spider silk enable forces arising from Laplace pressure differences and from surface energy gradients to combine so that hysteresis effects can be overcome and micrometre-sized water drops moved. Once the anisotropic structural features are damaged, spider silk fibres are no longer capable of directional water collection (Supplementary Figs 5–8).

In addition to enabling cooperation between two different driving forces, the structure of wet-rebuilt spider silk also optimizes hysteresis effects so as to favour the directional movement of water drops from joints to spindle-knots. These two regions have the same chemical composition, but different surface topographies that affect the spreading and movement of water drops. More specifically, a water drop will spread or move more readily along the parallel direction of an aligned surface topography than along a surface with a randomly rough topography^{25–27}. This is because the vapour–liquid–solid three-phase contact line (TCL) is continuous along the parallel direction of the surface with aligned topography and discontinuous on the randomly rough topography, with a continuous TCL allowing smooth spreading or moving of a liquid whereas a discontinuous TCL gives rise to more pronounced hysteresis effects^{1,25–27}. The joints in wet-rebuilt spider silk are comprised of relatively aligned nanofibrils that give rise to a fairly continuous TCL along the silk fibre axis, whereas the spindle-knots are comprised of random nanofibrils that cause the TCL to be discontinuous. Water drops moving along joints therefore experience

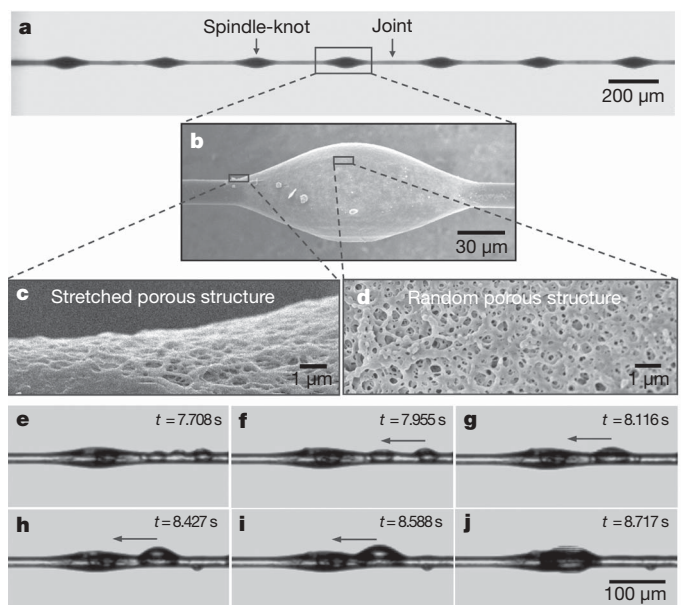


Figure 5 | Artificial spider silk that mimics the structure and water collection capability of natural spider silk. **a**, Optical image of spindle-knot/joint structure with periodicity of $394.6 \pm 16.1 \mu\text{m}$. **b–d**, SEM images of a spindle-knot (**b**), a stretched porous structure on the joint (**c**) and a random porous structure on the spindle-knot (**d**). **e–j**, Directional water collection on artificial spider silk. When the artificial spider silk is in mist at 0 s, tiny water drops randomly condense on the artificial spider silk at 7.708 s (**e**), and then directionally move from joint to spindle-knot with the volume increasing from 7.955 s to 8.717 s (**f–j**).

less hysteresis than those moving along spindle-knots, and this difference will further aid the movement of water drops from the joint to the spindle-knot.

Guided by the detailed mechanistic insights into directional water collection on spider silk gained in this study, we designed and fabricated artificial fibres that mimic the structural features of wet-rebuilt spider silk (see Supplementary Information for details). The optical image of this artificial spider silk (Fig. 5a) shows periodic spindle-knots that resemble those of the wetted spider silk and have a periodicity of $394.6 \pm 16.1 \mu\text{m}$. Spindle-knots and joints have diameters of $43.7 \pm 5.4 \mu\text{m}$ and $13.5 \pm 0.7 \mu\text{m}$ (Fig. 5b), respectively, and their microstructures are similar to those seen in wetted spider silk: the artificial joints have a stretched porous structure mimicking aligned nanofibrils (Fig. 5c), and the artificial spindle-knots exhibit random porous surface structures (Fig. 5d). The functional performance of the material is illustrated by the series of images in Fig. 5e–j. These show that when exposed to mist, small drops start to condense randomly on the artificial spider silk (Fig. 5e); and as the drop volume increases (Fig. 5f), water drops located on joints move towards spindle-knots (Fig. 5g–j). These observations clearly show that our artificial spider silk not only mimics the structure of wet-rebuilt spider silk but also its directional water collection capability. We therefore anticipate that the design principles uncovered and implemented in this study will aid the development of functional fibres for use in water collection and in liquid aerosols filtering in manufacturing processes.

Received 5 October; accepted 10 November 2009.

- Feng, L. *et al.* Super-hydrophobic surfaces: from natural to artificial. *Adv. Mater.* **14**, 1857–1860 (2002).
- Gao, X. F. & Jiang, L. Water-repellent legs of water striders. *Nature* **432**, 36 (2004).
- Blossey, R. Self-cleaning surfaces—virtual realities. *Nature Mater.* **2**, 301–306 (2003).
- Sun, T. L., Feng, L., Gao, X. F. & Jiang, L. Bioinspired surfaces with special wettability. *Acc. Chem. Res.* **38**, 644–652 (2005).
- Li, X. M., Reinhoudt, D. & Crego-Calama, M. What do we need for a superhydrophobic surface? A review on the recent progress in the preparation of superhydrophobic surfaces. *Chem. Soc. Rev.* **36**, 1350–1368 (2007).
- Parker, A. R. & Lawrence, C. R. Water capture by a desert beetle. *Nature* **414**, 33–34 (2001).
- Chaudhury, M. K. & Whitesides, G. M. How to make water run uphill. *Science* **256**, 1539–1541 (1992).
- Daniel, S., Chaudhury, M. K. & Chen, J. C. Fast drop movements resulting from the phase change on a gradient surface. *Science* **291**, 633–636 (2001).
- Daniel, S., Sircar, S., Gliem, J. & Chaudhury, M. K. Ratcheting motion of liquid drops on gradient surfaces. *Langmuir* **20**, 4085–4092 (2004).
- Lorenceanu, É. & Quéré, D. Drops on a conical wire. *J. Fluid Mech.* **510**, 29–45 (2004).
- Vollrath, F. & Porter, D. Spider silk as archetypal protein elastomer. *Soft Matter* **2**, 377–385 (2006).
- Vollrath, F. *et al.* Compounds in the droplets of the orb spider's viscid spiral. *Nature* **345**, 526–528 (1990).
- Liu, Y., Shao, Z. & Vollrath, F. Relationships between supercontraction and mechanical properties of spider silk. *Nature Mater.* **4**, 901–905 (2005).
- Vollrath, F. Strength and structure of spiders' silks. *Rev. Mol. Biotechnol.* **74**, 67–83 (2000).
- Vollrath, F. & Edmonds, D. T. Modulation of the mechanical properties of spider silk by coating with water. *Nature* **340**, 305–307 (1989).
- Edmonds, D. T. & Vollrath, F. The contribution of atmospheric water vapour to the formation and efficiency of a spider's capture web. *Proc. R. Soc. Lond. B* **248**, 145–148 (1992).
- Backer, N. *et al.* Molecular nanosprings in spider capture-silk threads. *Nature Mater.* **2**, 278–283 (2003).
- Peter, H. M. The spinning apparatus of Uloboridae in relation to the structure and construction of capture threads (Arachnida, Araneida). *Zoomorphology* **104**, 96–104 (1984).
- Porter, D. & Vollrath, F. Nanoscale toughness of spider silk. *Nanotoday* **2**, 6 (2007).
- Emile, O., Floch, A. L. & Vollrath, F. Biopolymers: shape memory in spider draglines. *Nature* **440**, 621 (2006).
- Yang, J., Yang, Z., Chen, C. & Yao, D. Conversion of surface energy and manipulation of a single droplet across micropatterned surfaces. *Langmuir* **24**, 9889–9897 (2008).
- Fang, G., Li, W., Wang, X. & Qiao, G. Droplet motion on designed microtextured superhydrophobic surfaces with tunable wettability. *Langmuir* **24**, 11651–11660 (2008).
- Wenzel, R. N. Resistance of solid surface to wetting by water. *Ind. Eng. Chem.* **28**, 988–994 (1936).
- Quéré, D. Wetting and roughness. *Annu. Rev. Mater. Res.* **38**, 16.1–16.29 (2008).
- Zheng, Y. M., Gao, X. F. & Jiang, L. Directional adhesion of superhydrophobic butterfly wings. *Soft Matter* **3**, 178–182 (2007).
- Gau, H., Herminghaus, S., Lenz, P. & Lipowsky, R. Liquid morphologies on structured surfaces: from microchannels to microchips. *Science* **283**, 46–49 (1999).
- Yoshimitsu, Z., Nakajima, A., Watanabe, T. & Hashimoto, K. Effects of surface structure on the hydrophobicity and sliding behavior of water droplets. *Langmuir* **18**, 5818–5822 (2002).

Supplementary Information is linked to the online version of the paper at www.nature.com/nature.

Acknowledgements We thank the State Basic Research Program of China (2007CB936403), the Key Program in the National Natural Science Foundation of China (119030601101), and the Knowledge Innovation Program in the Chinese Academy of Sciences (2A20052222200301).

Author Contributions Y. Zheng, H.B., Z.H. and X.T. performed the experiments. Y. Zheng and Z.H. worked on the water collection of natural spider silks, H.B. and X.T. worked on the fabrication and water collection of artificial spider silk. Y. Zheng and H.B. conducted the control experiments. Y. Zheng, H.B., Y. Zhao and L.J. collected and analysed the data and proposed the mechanism of directional water collection on spider silk. Y. Zheng, F.-Q.N., Y. Zhao, J.Z. and L.J. wrote the text. L.J. conceived the project and designed the experiments.

Author Information Reprints and permissions information is available at www.nature.com/reprints. The authors declare no competing financial interests. Correspondence and requests for materials should be addressed to L.J. (jjanglei@iccas.ac.cn) or Y. Zhao (zhaoyong@iccas.ac.cn).